Archive of Applied Mechanics 67 (1996) 68–80

Analysis of long torsional strings by proper orthogonal decomposition

E. Kreuzer, O. Kust

Summary Nonlinear excitations cause angular vibrations in torsional strings. In long strings, the vibrations are characterized by different dynamic behavior over the length. For a general case of a long torsional string, a simplified mathematical model is introduced and numerically simulated. In order to gain insight into the complex spatio-temporal dynamics, the method of proper orthogonal decomposition is applied. A short description of this powerful technique for continuous as well as discrete systems follows. By proper orthogonal decomposition, the dynamic response is projected on a subset of the state space in which the most dominant dynamic effects take place. The time-invariant eigenfunctions represent the most persistent structures in the system. By this method the eigenfunctions of long torsional strings are investigated. The reduction of the system's dimension as well as the approximation of the system state is presented.

Key words torsional strings, vibrations, proper orthogonal decomposition, eigenfunctions, system dimension reduction

1 Introduction

In many technical systems, torsional strings serve as power-transmission elements between the drive and the output. Examples are drive shafts in cars and ships and drill strings for deep drilling. Torsional vibrations are often caused by nonlinearities in the string. In the case of long torsional strings, wave reflections appear and the moment of inertia can no longer be neglected. Long torsional strings are represented in mechanical modeling by a continuous one-dimensional body with oscillations depending on time and position, and mathematically expressed by partial differential equations. Often, boundary conditions are given by the velocity at the drive and, in general, by a nonlinear torque at the output. Due to the nonlinearity, self-excited vibrations can occur. These vibrations are highly unwelcome, because they may cause disruption or, in severe cases, even damage the transmission element.

Vibrations in long torsional strings result in spatio-temporal signals. For their analysis, well-known methods are Galerkin approximations or Fourier series. Especially in linear cases and for systems with fixed or harmonic boundary conditions, these methods are appropriate, particularly if the shapes of the ansatzfunctions or of the eigenmodes are approximately known. If the signals are complex and the ansatzfunctions are not obvious, experience or luck is necessary in their choice. One method to gain insight into the dynamics without the prior knowledge of the eigenmodes and ansatzfunctions, especially in nonlinear cases, is the proper orthogonal decomposition (POD) of the signals.

In the present paper, we first introduce a general system of a long torsional string. Then the mathematical model will be formulated. The simulation and the behavior for different values of a characteristic system parameter will be shown through bifurcation analysis. Then, an introduction to the proper orthogonal decomposition for continuous functions as well as discrete signals will be given, and the relationship between them shown. The theoretical description will be followed by analytical and numerical investigations of a torsional string of a real system. We will demonstrate how the complex system state can be understood in a simpler manner, how the dimension of the system can be reduced efficiently, and how the POD can be used for approximation.

Received 12 February 1996; accepted for publication 19 June 1996

E. Kreuzer, O. Kust
Technical University Hamburg-Harburg, Eißendorfer Straße 42,
D-21071 Hamburg, Germany

2 Modeling

A simplified model of a long torsional string between the drive and the output is shown in Fig. 1. A string of length l is driven on its left end at $x = 0$, and loaded by an external torque T. The moment of inertia Θ of a disc (e.g. a cog-wheel, flywheel or break) is located at its other end at $x = l$. Often, the angular velocity at the drive ω_0 will be given. Characteristic parameters of the long string are the density ρ, the shear module G, the polar moment of area I_p, inner and outer damping coefficients d_i and d_a, respectively and the applied torque per unit length $m(x)$.

As an example for long torsional strings, we consider a drill string for drilling deep holes for the exploration and production of oil and gas, as illustrated in Fig. 2. The drill string consists of tubes, and lengths up to 5000 meters are common. Therefore, drill strings are very slender structures. The upper end of the drill string is held by a hoisting in the derrick. The rotary table, a large horizontal gear wheel which is driven by an electric or hydraulic motor, transfers the rotary motion to the drill pipes and the bit. Drill collars are heavy, thick-walled pipes destinated to transfer load to the bit, and to produce tension in the drill pipes, which otherwise would bend.

The drill string will be considered as a one-dimensional elastic body. Due to the large torsional stiffness of the drill collars in relation to the drill pipes, the drill collars will be modeled as a rigid body at the lower end of the drill pipes. In a first approximation, the drill string can be represented by the string introduced above.

Equation of motion By visualizing the equilibrium of an infinitesimal thin disk of a torsional string, its dynamics can be described by the following partial differential equation (PDE)

$$\rho I_p \ddot{\varphi} + d_a \dot{\varphi} - G I_p \varphi'' - d_i G I_p \dot{\varphi}'' = m(x,t), \quad x \in \Omega = [0,l], \tag{1}$$

with $(\dot{}) = \partial/\partial t$ and $()' = \partial/\partial x$ denoting the derivatives with respect to time and position. The boundary conditions are given by the rotational velocity ω_0 at the drive; in our example this is the velocity of the rotary table at the upper end, and the applied torque and the angular momentum of the disc at the other end

$$\partial\Omega: \begin{cases} x = 0: & \dot{\varphi}(0,t) = \omega_0(t), \\ x = l: & G I_p [\varphi'(l) + d_i \dot{\varphi}'(l)] = -T[\varphi(l), \dot{\varphi}(l)] - \Theta \ddot{\varphi}(l). \end{cases} \tag{2}$$

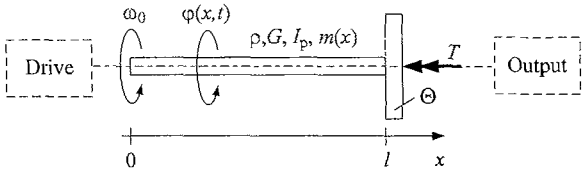

Fig. 1. Torsional string

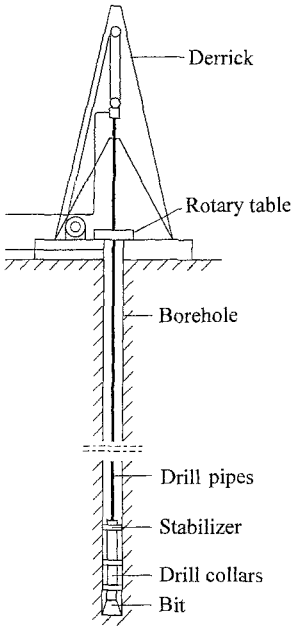

Fig. 2. Drilling platform, borehole, and drill string for producing oil and gas

In our system, the applied torque consists of the torque on the bit and the angular momentum of the drill collars and the bit. The bit torque depends nonlinearly on the angular velocity of the bit $\dot{\varphi}(l) = \dot{\varphi}_{bit}$ by means of the friction and the shearing during the rock cutting as well as on the angular position of the bit $\varphi(l) = \varphi_{bit}$ due to longitudinal oscillations of the string excited every revolution. Therefore, the load on the bit increases and decreases with every turn

$$T = \tfrac{1}{2}(1 + \cos\varphi_{bit})\, T_0(\dot{\varphi}_{bit}). \tag{3}$$

The nonlinear function T_0 (full load on the bit) depends on the velocity of the bit and is shown in Fig. 3.

Simulation For some types of excitation, like fixed and free boundaries, the PDE equation of motion given by Eq. (1) can be solved directly, but normally there is no analytical solution available for a nonlinear boundary condition. Furthermore, only for special cases solving routines are implemented in software packages. In order to solve the PDE, the spatial domain Ω will be discretized via n space points (nodes) and $n-1$ intervals of length $\Delta x = l/(n-1)$ each

$$x \to x_i, \quad \varphi \to \varphi_i, \quad i = 1,\ldots,n. \tag{4}$$

Using central differences for the spatial derivatives and expanding the spatial derivatives on the boundary nodes with a third-order Taylor series, we get a set of differential equations for the nodes

$$\ddot{\varphi}_i = f_i(\varphi_j, \dot{\varphi}_k), \quad i,j,k = 1,\ldots,n, \tag{5}$$

where $\varphi_1 \equiv \alpha_0 = \varphi_{rt}$ denotes the angle at the drive (rotary table), and $\varphi_n \equiv \varphi_{bit}$ is the angle at the output (the bit in this example). The truncating error over the whole domain is of order $\mathcal{O}(\Delta x^3)$. For more details on the numerical solution of PDEs we refer to [13], [15].

Transforming all second-order ODEs into a set of first-order ODEs, the complete set of equations of motion is given by

$$\dot{\mathbf{x}} = \mathbf{A}(\mu)\mathbf{x} + \mathbf{f}(\mathbf{x},\mu), \quad \mathbf{x} = [\varphi^T \dot{\varphi}^T]^T \in \mathbb{R}^{2n}, \quad \boldsymbol{\varphi} = [\varphi_i], \quad i = 1,\ldots,n, \tag{6}$$

with A and f denoting the linear and nonlinear part of the system. Parameter μ is employed to enable a variation of characteristics such as the angular velocity ω_0 of the drive or the length l of the string. Finally, the initial-value problem is solved with a standard variable-order variable-step routine. The result is the dynamic flow $\boldsymbol{\Phi}_t(\bullet): \mathbb{R}^{2n} \to \mathbb{R}^{2n}$ of the system at the discrete space points x_i, $i = 1, \ldots, n$.

There are several possible ways to represent the flow of the system:

- Time plots, depicting the velocity with respect to time at every location x_i. In Fig. 4 time plots are shown for the drive (rotary table), the output (bit) and a level between them. Due to the unbounded increase of the angles with time, such a representation of the angles is not appropriate.
- Cylindrical state space: the angles φ_i increase with time, and they are unbounded. On the other hand, they are periodical with a period of 2π. In order to overcome the unbounded system state, the tra-

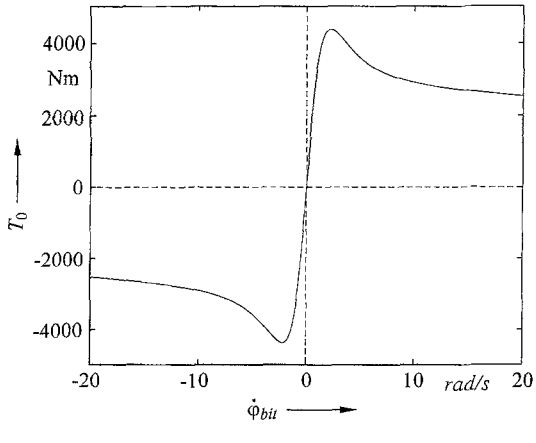

Fig. 3. Torque characteristic on bit

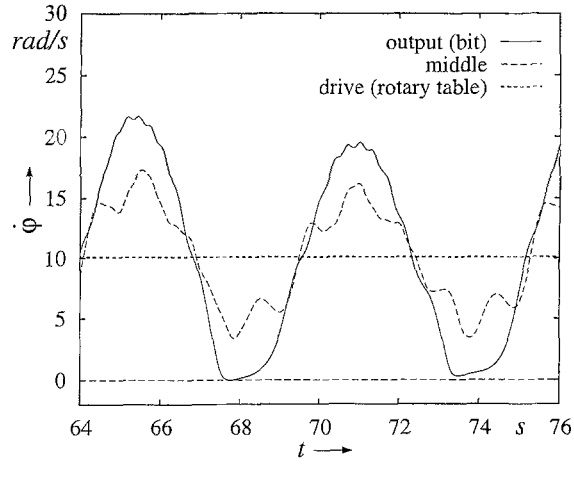

Fig. 4. Time plots of the velocities at several levels

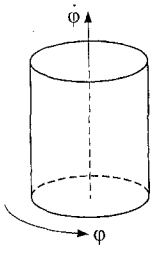

Fig. 5. Cylindrical state space

jectories of each space point can be represented in a cylindrical state space by the following mapping, Fig. 5:

$$(t, \varphi_i, \dot{\varphi}_i) \in \mathbb{R} \times \mathbb{R} \times \mathbb{R} \to (\psi_i, \dot{\varphi}_i) \in S \times \mathbb{R}, \quad \psi_i = \varphi_i \bmod 2\pi. \tag{7}$$

Unwinding the surface of the cylindrical state space, the state space becomes a rectangular one. Its width of 2π represents the angle φ and its height corresponds to the angular velocity $\dot{\varphi}$, Fig. 6.

- Rotating coordinate system (Fig. 7): if there exists a bounded phase difference between the space locations, the state space will be represented in a system rotating with a cross section at an arbitrary space point k

$$(t, \varphi_i, \dot{\varphi}_i) \to (t, \phi_i, \dot{\phi}_i), \quad \phi_i = \varphi_i - \varphi_k, \quad i = 1, \ldots, n. \tag{8}$$

Due to the fact that now only relative coordinates are considered, there is a loss of information: the angle and the angular velocity of the k-th component is equal to zero, $\phi_k \equiv 0, \quad \dot{\phi}_k \equiv 0$.

Bifurcations In real technical systems, torsional vibrations can often be observed. Such vibrations in drill strings have been well-known for a long time, [4]. They are highly unwelcome, and in severe cases they can even damage the string.

The variation of the parameters of the system will lead to various flows. The investigation of the influence of these parameters, for example, the velocity of the drive (rotary table) $\mu = \omega_0 = \omega_{rt}$, shows that periodic as well as chaotic behavior can occur. In Fig. 8 the trajectories of the bit are depicted for different velocities of the drive in a typical range of practicably relevant velocities. For $\omega_0 = 10.1$ rad/s and $\omega_0 = 11.0$ rad/s, the bit performs different periodic motions while for $\omega_0 = 11.6$ rad/s chaotic behavior appears.

The pictures are *not* phase plots in original sense. The overlapping of the trajectories results in the projections of the whole state space on a single 2-D state space.

An appropriate way to investigate qualitative changes characterized by bifurcations is the method of Poincaré mapping, [9]. A bifurcation diagram for the varying angular velocity of the drive is shown in Fig. 9. It illustrates the intersection points of the trajectory of the bit with the Poincaré plane $\Sigma = \{\varphi_{bit} -$

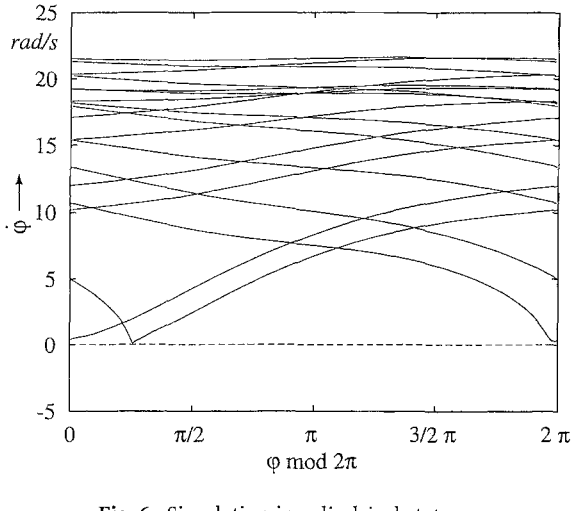

Fig. 6. Simulation in cylindrical state space

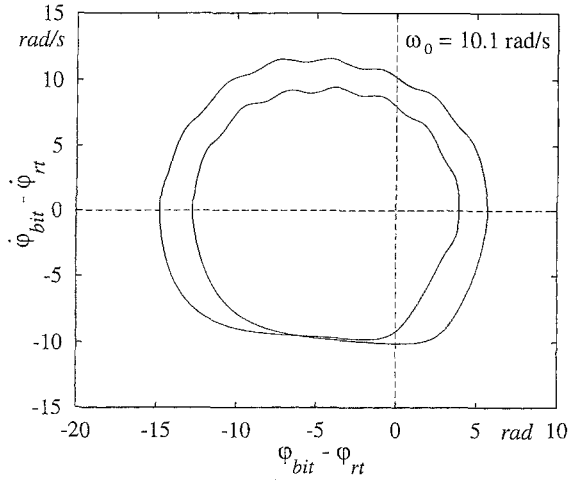

Fig. 7. Phase portrait of the bit trajectory in a coordinate frame rotating with the rotary table (index *rt*)

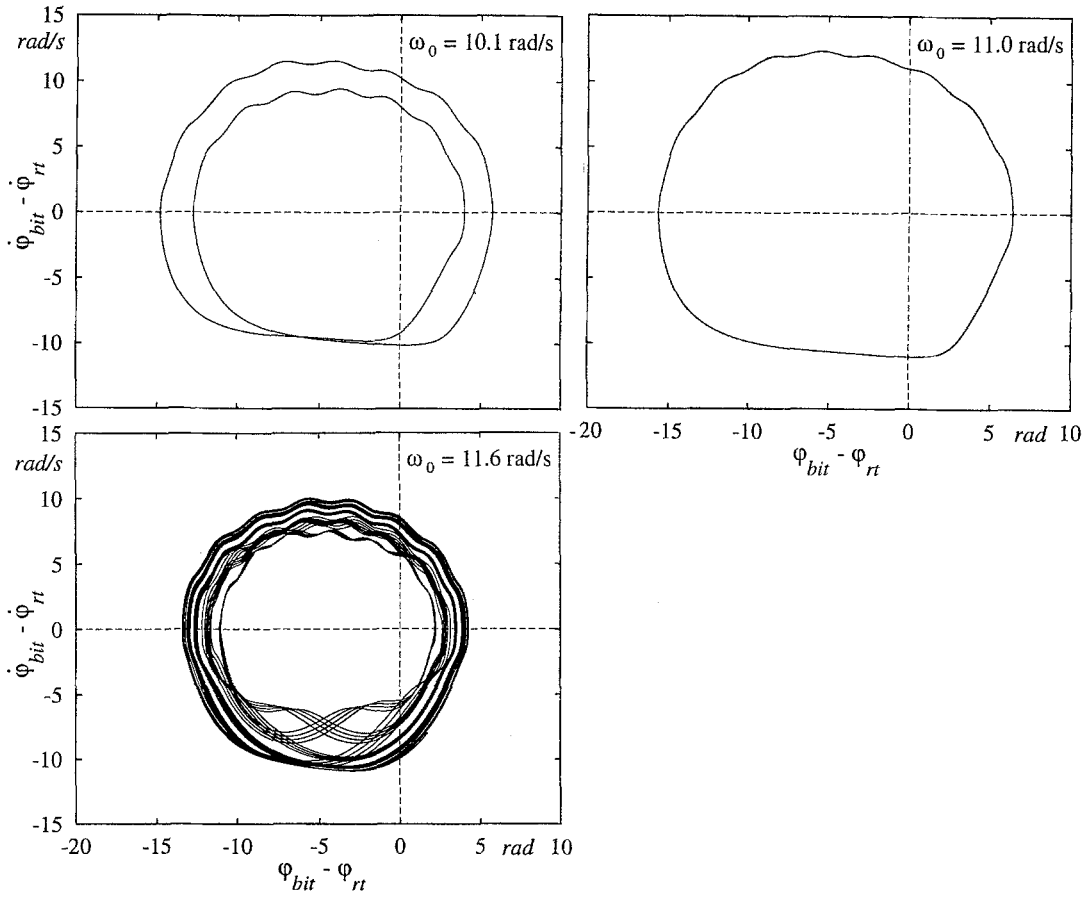

Fig. 8. Trajectory of the bit for different values of the angular velocity ω_0 of the drive

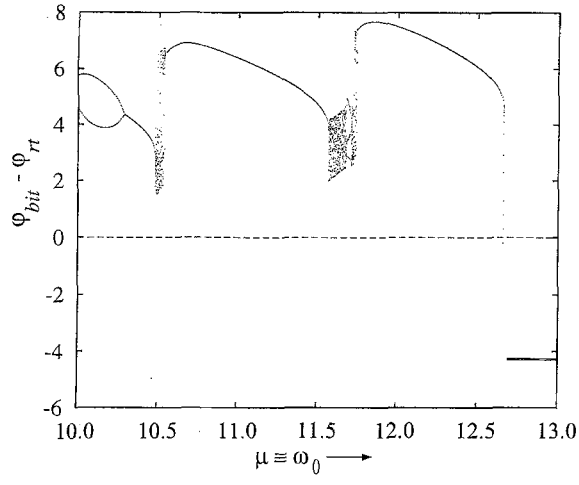

Fig. 9. Poincaré map of the trajectory of the bit depending on the velocity of the drive ω_0

$\varphi_{rt} | \dot{\varphi}_{bit} - \omega_0 = 0 \wedge \varphi_{bit} - \varphi_{rt} > 0\}$ depicted against the increasing bifurcation parameter μ which represents the angular velocity ω_0 of the bit in a typical range of velocities. For the value $\omega_0 = 10.1$ rad/s two intersection points occur, for $\omega_0 = 11.0$ rad/s one, and for $\omega_0 = 11.6$ rad/s the chaotic motion manifests in infinitely many points. For velocities greater than 12.6 rad/s the vibrations vanish, and a stable rotation with fixed phase difference between bit and rotary table occurs.

3
Proper orthogonal decomposition

For the analysis of the spatio-temporal dynamics, proper orthogonal decomposition (POD), which is often also called Karhunen-Loève (KL) transformation, has been recently used as an efficient tool in several disciplines.

POD goes back to [10], [11] and [6], [7], and has been successfully employed for the analysis of dynamical systems by several researchers, see e.g. [12], [2], [3], [8], [1] and others. POD is used in the context of turbulence, picture recognition, data compression and chemistry.

With proper orthogonal decomposition, the spatio-temporal dynamics will be projected on a subset of the solution space in which the most dominant dynamics take place. The time-invariant eigenfunctions represent the most persistent structures in the system, while the corresponding amplitudes are uncorrelated. Nontypical patterns, like noise in the dynamics, are faded out. The variance of a time function serves as a measure for its dominance. For appplying POD, no a-priori knowledge of the system and no ansatzfunctions are necessary, and often the dynamics can be approximated very well by only a few eigenfunctions. Due to this fact, an efficient reduction of the system's dimension can be reached.

Continuous functions Spatio-temporal dynamics may be given by the continuous function $u(x, t)$ in space and time. In order to gain insight into the dynamics, we are interested in coherent time-independent structures of the signal. The structures are manifolds, on which the most part of the kinetic energy is stored in a time average. On these manifolds, the system state rests with major variance. Let the function be of the class of square integrable functions on the interval $[a, b]$, $u \in L^2[a, b]$. In physical terms, the kinetic energy of such systems is bounded.

The space U in which the dynamics of the system takes place can be decomposed into the two linear subspaces U_1 and U_2 as the direct sum $U = U_1 \oplus U_2$, [14]. For the projection of an element $u \in U$ onto the two subspaces holds, that $u = u_1 + u_2$ with $u_1 \in U_1$ and $u_2 \in U_2$, Fig. 10.

In this way, the function u will be projected onto the subspace $U^{(\nu)} = \operatorname{span}\{\psi_1, \ldots, \psi_\nu\}$ being the space spanned by ν functions $\psi_1, \ldots, \psi_\nu$ of a set of orthonormal square integrable basis functions $\{\psi_i\}_{i \in \mathbb{N}} \in L^2[a, b]$

$$u^{(\nu)} = \sum_{i=1}^{\nu} (u, \psi_i) \psi_i, \tag{9}$$

where

$$(u, v) = \int_a^b u(x, t)\, v(x, t)\, dx, \tag{10}$$

denotes the inner product of the functions u and v defined on the interval $[a, b]$. The basis functions will be a set of orthonormal functions

$$\int_a^b \psi_i(x) \psi_j(x)\, dx = \delta_{ij}, \quad \delta_{ij} = \begin{cases} 0, & i \neq j, \\ 1, & i = j. \end{cases} \tag{11}$$

We understand "coherent structures" as the functions which are most similar to the members of $u(x)$ on the average, or, in other words, they will represent the mean "energy" of the signal u projected on the basis functions ψ_i

$$\lambda_i = \lim_{T \to \infty} \left\{ \frac{1}{T} \int_0^T [(\psi_i, u(x, t))]^2\, dt \right\}, \quad i = 1, 2, \ldots. \tag{12}$$

With respect to the inner product (10) Eq. (12) leads to the integral equation

$$\lambda_i = ((K(x, y), \psi_i(y)), \psi_i(x)), \tag{13}$$

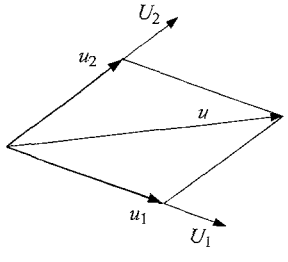

Fig. 10. Decomposition of U into the two linear subspaces U_1 and U_2 as the direct sum $U = U_1 \oplus U_2$. Projection of an element $u \in U$ onto the two subspaces, such that $u = u_1 + u_2$ with $u_1 \in U_1$ and $u_2 \in U_2$

with the semi-positive definite kernel

$$K(x,y) = \lim_{T\to\infty} \frac{1}{T}\int_0^T u(x,t)\,u(y,t)\,dt. \tag{14}$$

Considering the orthogonality condition Eq. (11) results in the Fredholm integral equation

$$\int_a^b K(x,y)\,\psi_i(y)\,dy = \lambda_i \psi_i(x). \tag{15}$$

Sorting the eigenfunctions ψ_i with descending eigenvalues λ_i,

$$\lambda_1 \geq \lambda_2 \geq \cdots \geq \lambda_\nu \geq \cdots \geq 0, \tag{16}$$

which corresponds to the ordering of the variances of the eigenfunctions ψ_i, the eigenfunctions represent the manifolds from most to least dominance.

Due to the fact that the eigenfunctions span a subspace in which the dynamics takes place, every function u within this subspace can be represented as a combination of the eigenfunctions. Therefore, the system state can be approximated by a summation of the first ν eigenfunctions ψ_i weighted with time-depending amplitudes $a_i(t)$

$$u^{(\nu)} = \sum_{i=1}^{\nu} a_i(t)\,\psi_i(x). \tag{17}$$

For the time functions $a_i(t)$ hold from Eqs. (17), (9) and (10)

$$a_i(t) = \int_a^b u(x,t)\,\psi_i\,dx. \tag{18}$$

The convergence of the series (17) for $\nu \to \infty$ is given by Parseval's equation: multiplying both sides of (17) with u and integrating afterwards over the domain [a, b] leads to

$$\int_a^b u^2(x)\,dx = \sum_{i=1}^{\infty} a_i^2. \tag{19}$$

From Eq. (13) together with Eqs. (14) and (11), we get the important property of the time functions $a_i(t)$

$$\lim_{T\to\infty} \frac{1}{T}\int_0^T a_i(t)\,a_j(t)\,dt = \lambda_i \delta_{ij}. \tag{20}$$

The time functions are uncorrelated. The eigenvalue λ_i of an eigenfunction ψ_i is a measure for the variance of the system state projected onto this eigenfunction.

Given two orthonormal sets $\{\psi_k\}$ and $\{\phi_k\}$, with

$$u(x,t) = \sum_{k=1}^{\nu} a_k(t)\,\psi_k(x), \tag{21}$$

investigated by POD, and

$$u(x,t) = \sum_{k=1}^{\nu} b_k(t)\,\phi_k(x), \tag{22}$$

$\{\phi_k\}$ being any other orthonormal basis, then the following relation is obtained:

$$\sum_{k=1}^{\nu} \langle a_k^2 \rangle = \sum_{k=1}^{\nu} \lambda_k \geq \sum_{k=1}^{\nu} \langle b_k^2 \rangle, \quad \forall \nu, \tag{23}$$

where $\langle \bullet \rangle$ denotes the time average. For all ν more energy is stored in the first ν eigenfunctions of the POD than in any other eigenfunctions. That is the optimality condition of the Karhunen-Loève transformation.

Discrete functions The given data set $u_i(t) = u(x_i, t)$ can be split into a mean part $\bar{\mathbf{u}}$ and a second part $\boldsymbol{\eta}$ with zero-time average. Then the signals have the following properties:

$$\mathbf{u}(t) = [u_1(t),\ldots,u_n(t)]^T = \bar{\mathbf{u}} + \boldsymbol{\eta}(t), \quad \mathbf{u},\bar{\mathbf{u}},\boldsymbol{\eta} \in \mathbb{R}^n, \quad \mathbf{E}(\mathbf{u}) = \bar{\mathbf{u}}, \quad \mathbf{E}\{\boldsymbol{\eta}\} = \mathbf{0}, \tag{24}$$

thereby $\mathbf{E}\{\bullet\}$ denotes the time average of its argument. As in the continuous case, a linear projection P of $\boldsymbol{\eta}$ onto a subspace with orthonormal basis $\{\boldsymbol{\psi}_1,\ldots,\boldsymbol{\psi}_n\}$ is given by

$$P\boldsymbol{\eta} = \sum_{i=1}^{n} (\boldsymbol{\psi}_i, \boldsymbol{\eta})\boldsymbol{\psi}_i, \tag{25}$$

where $(\bullet,\bullet)$ denotes the inner or scalar product of two vectors. The data set can be expanded by the series

$$\mathbf{u} = \bar{\mathbf{u}} + \sum_{i=1}^{n} a_i(t)\boldsymbol{\psi}_i. \tag{26}$$

For the time functions $a_i(t)$ hold from (25)

$$a_i = (\boldsymbol{\psi}_i, \boldsymbol{\eta}) = \boldsymbol{\psi}_i^T \boldsymbol{\eta} = \boldsymbol{\psi}_i^T (\mathbf{u} - \bar{\mathbf{u}}). \tag{27}$$

The data set can be written in matrix notation with $\mathbf{a} = [a_1(t),\ldots,a_n(t)]^T$, $\boldsymbol{\Psi} = [\boldsymbol{\psi}_1,\ldots,\boldsymbol{\psi}_n]$ as

$$\mathbf{u}(t) = \bar{\mathbf{u}} + \boldsymbol{\Psi}\mathbf{a}(t), \quad \boldsymbol{\Psi} \in \mathbb{R}^{n\times n}, \mathbf{a},\mathbf{u},\bar{\mathbf{u}} \in \mathbb{R}^n. \tag{28}$$

It is the aim of the KL-transformation to find the basis vectors in such a way that the corresponding time functions are uncorrelated. Assuming $\mathbf{E}\{\mathbf{a}\} = \mathbf{0}$ means all covariances of $\mathbf{a}$ vanish, and the covariance matrix becomes diagonal:

$$\mathbf{C}_{aa} = \mathbf{C}_{aa}^T = \mathbf{E}\{(\mathbf{a} - \mathbf{E}\{\mathbf{a}\})(\mathbf{a} - \mathbf{E}\{\mathbf{a}\})^T\} = \mathbf{E}\{\mathbf{a}\mathbf{a}^T\} = \mathbf{diag}\{\lambda_1,\ldots\lambda_n\}. \tag{29}$$

In order to determine a basis $\boldsymbol{\Psi}$, the second moment $\mathbf{E}\{\mathbf{u}\mathbf{u}^T\}$ of the data $\mathbf{u}$ is calculated. Using (28), (29) and $\mathbf{E}\{\mathbf{a}\} = \mathbf{0}$ this leads to

$$\mathbf{E}\{\mathbf{u}\mathbf{u}^T\} = \bar{\mathbf{u}}\bar{\mathbf{u}}^T + \boldsymbol{\Psi}\mathbf{C}_{aa}\boldsymbol{\Psi}^T. \tag{30}$$

Together with rules for calculating covariance matrices

$$\mathbf{C}_{uu} = \mathbf{E}\{\mathbf{u}\mathbf{u}^T\} - \mathbf{E}\{\mathbf{u}\}\mathbf{E}\{\mathbf{u}^T\} = \mathbf{E}\{\mathbf{u}\mathbf{u}^T\} - \bar{\mathbf{u}}\bar{\mathbf{u}}^T = \boldsymbol{\Psi}\mathbf{C}_{aa}\boldsymbol{\Psi}^T \tag{31}$$

and the properties of orthonormal vectors

$$\boldsymbol{\psi}_i^T\boldsymbol{\psi}_j = \delta_{ij} \rightarrow \boldsymbol{\Psi}^T\boldsymbol{\Psi} = \mathbf{E}, \tag{32}$$

we obtain an eigenvalue problem for the basis vectors $\boldsymbol{\psi}_i$

$$(\mathbf{C}_{uu} - \lambda_i\mathbf{E})\boldsymbol{\psi}_i = \mathbf{0}, \quad i = 1,\ldots,n, \tag{33}$$

where $\mathbf{E}$ denotes the $n \times n$ identity matrix. Using the fact that the covariance matrix $\mathbf{C}_{uu}$ of the data set is real, symmetric and of order n, there exist exactly n real eigenvalues with n corresponding real orthogonal eigenvectors $\boldsymbol{\psi}_i$. Sorting the eigenvalues in decreasing order, $\lambda_1 \geq \lambda_2 \geq \cdots \geq \lambda_n$, the eigenfunction $\boldsymbol{\psi}_1$ represents the most persistent spatial structure corresponding to a time function $a_1(t)$ with greatest variance.

For dynamic systems, the phase space can be approximated by the first v eigenfunctions as the sum

$$\tilde{\mathbf{u}}^{(v)} = \bar{\mathbf{u}} + \sum_{i=1}^{v} a_i\boldsymbol{\psi}_i. \tag{34}$$

We introduce the approximation error $\varepsilon^{(v)}$ depending on the number v of used eigenfunctions,

$$\varepsilon^{(v)} = \lim_{T\to\infty} \int_0^T \| \mathbf{u} - \tilde{\mathbf{u}}^{(v)} \|_2 \, dt. \tag{35}$$

For the choice of v, a practical condition is given with the error limit δ by

$$v = \{v | \varepsilon^{(v)} \leq \delta\}. \tag{36}$$

With formulation (34), the complex set of data can be understood in a simpler manner and, moreover, due to $v < n$, it can be used for storing the set efficiently. For an approximation with K eigenvectors ψ for M time steps and n space points, we use one average vector $\bar{u}$ of dimension n, v eigenvectors ψ_i of dimension n each, and $v \cdot M$ timefunctions a_i. For storing all time steps in all locations, we need $n \cdot M$ storage places. For a very large number of time steps, the relation of the storing place is n/v.

Relationship between continuous and discrete eigenfunctions From the discretization of the interval $x \in \Omega = [a,b]$ into a set of points $x \to x_i, i = 1,\ldots,n$, it follows, that the eigenvector $\psi = [\psi_1,\ldots,\psi_n]^T \in \mathbb{R}^n$ describes the continuous eigenfunction $\psi(x)$ only at the n points x_i. Furthermore, by applying the inner product, the orthogonality condition holds only for these points x_i.

To bring the eigenvector and the continuous eigenfunction into line, the eigenvector ψ must be scaled, Fig. 11

$$\tilde{\psi} = \kappa \psi. \tag{37}$$

The linear scaling factor κ can be obtained in the first approximation from the comparison of Eqs. (18) and (27), by applying rectangular rule κ_{rect} or trapezoidal rule κ_{trap} for the integration

$$\kappa_{rect} = \frac{1}{\sqrt{\Delta x \sum_{i=1}^{n-1} \psi_i^2}}, \quad \kappa_{trap} = \frac{1}{\sqrt{\Delta x \left[\frac{1}{2}\psi_1^2 + \sum_{i=2}^{n-1} \psi_i^2 + \frac{1}{2}\psi_n^2\right]}}. \tag{38}$$

Furthermore, there exists a great variety of algorithms for a quadrature of a function. Representing the eigenfunction with polynomials

$$\psi = [\psi_i] \to p(x) = \sum_{k=0}^{m} a_m x^m, \tag{39}$$

the eigenfunction can be approximated by the scaled eigenfunction $\tilde{\psi}$

$$\tilde{\psi}(x) = \frac{p(x)}{\sqrt{\int_a^b p^2(x)\,dx}}. \tag{40}$$

For many applications, no scaling of the eigenvectors will be necessary due to the linearity of the scaling. It will be only used in cases when a continuous function is necessary, i.e. for projections from discrete eigenvector.

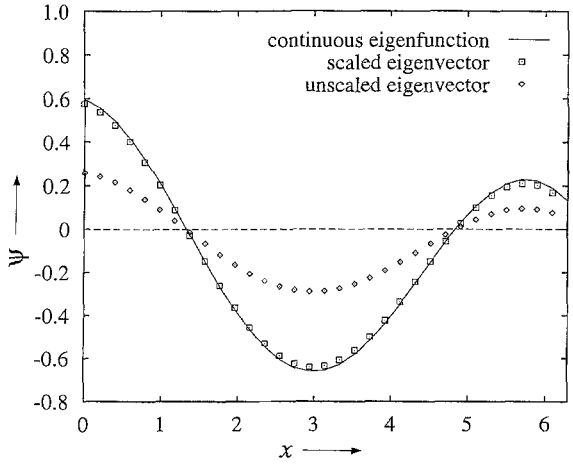

Fig. 11. Continuous eigenfunction, eigenvector ψ and scaled eigenvector $\tilde{\psi}$

4
Analysis of torsional vibrations by proper orthogonal decomposition

As announced in Sec. 2, the equation of motion (1) will be solved with regards to the boundary conditions given in (2). The results are time series of the angles φ_i and angular velocities $\dot{\varphi}_i$ of the nodal points x_i, $i = 1,\ldots,n$. For applying the POD on the data set we must take into account that the values of the angles are unbounded, and a decomposition would not work as introduced in Sec. 3. Therefore, we analyze the system state in a co-rotating coordinate system as mentioned above. The loss of information by means of a rotating frame can be accepted, because we are interested only in the torsional *vibrations* and not in the mean motion of the system. In many technical systems, the mean motion is given or desired, and only differences are of interest.

The set of equations of motion (6) can be rewritten with respect to a co-rotating coordinate frame which is fixed with the drive

$$\dot{\mathbf{u}} = \mathbf{A}^*\mathbf{u} + \mathbf{f}^*(\mathbf{u}), \quad \mathbf{u}(0) = \mathbf{u}_0, \tag{41}$$

with $\mathbf{A}^*$ and $\mathbf{f}^*$ denoting the linear and nonlinear term, respectively. The flow of the new system state is $\mathbf{\Phi}_t^*(\mathbf{u}_0)$. After solving the initial boundary value problem (41), we get a data set $\mathbf{u}$ of the torsional vibrations with the following property:

$$\mathbf{u} = [0,(\varphi_i - \varphi_{rt}),0,(\dot{\varphi}_i - \dot{\varphi}_{rt})]^T, \quad i = 2,\ldots,n, \quad \mathbf{u}\in\mathbb{R}^{2n}. \tag{42}$$

Due to the two zero rows $u_1 \equiv 0$ and $u_{n+1} \equiv 0$, two zero rows and two zero columns occur in the covariance matrix $\mathbf{C}_{uu}$. Therefore, the rank of the covariance matrix is

$$\operatorname{rank}(\mathbf{C}_{uu}) = 2n - 2, \tag{43}$$

instead of full rank $2n$. Additionally, in practice, the covariance matrix is often numerically nearly singular. For calculating the eigenvectors and eigenvalues, we use singular value decomposition (SVD), [5].

The drill string was discretized by $n = 65$ space points and $2n = 130$ ODEs, respectively. Totally, approx. 6000 time steps have been calculated. Applying the POD on the data set $\mathbf{u}$, we obtain eigenvectors $\boldsymbol{\psi}_i$ and time functions $a_i(t)$, $i = 1,\ldots,2n$. The first six eigenvectors are shown in Fig. 12 for $\omega_0 = 10.1$ rad/s and a length of the drill string of 2000 m (they correspond to the phase plot Fig. 8). The first eigenvector points in the direction of the velocity with the most persistence, the second in the direction of the most persistent angle. From the shape of the sixth eigenvector, it follows that there exists more than one point having the same sixth eigenmode, while the other eigenmodes are only concurrent in the point $x = 0$ at the drive.

In comparison to other methods, like Galerkin expansion or Fourier series, it is obvious how powerful POD is. Eigenvectors as well as eigenvalues (see below) were directly determined out of the correlation of the flow of the system by means of a mathematical measure.

The PDE (1) is linear but the boundary conditions (2) are nonlinear. Due to the excitation lying not nearby an eigenfrequency of the system, the following can be observed: the calculation of the eigenvectors and time functions for different values of the bifurcation parameter μ (here it is the angular velocity ω_0 of the drive) yields the eigenvectors which are almost constant, while the time functions $a_i(t)$ change qualitatively with μ, Fig. 13.

From (34) it follows that the data set $\mathbf{u}$ could be approximated by the first v eigenvectors. Figure 14 shows the attractor of the bit trajectory, the directions of the first two eigenvectors projected on the state space of the bit, and the approximation of the attractor by the first four eigenvectors in a co-rotating coordinate frame for a drive speed of $\omega_0 = 10.1$ rad/s. The good approximation by means of only a few eigenvectors is obvious.

The eigenvalues λ_i of the eigenvectors $\boldsymbol{\psi}_i$ decrease exponentially down to some limit (approximately the machine unit) with the first 20 eigenvectors, and then remain nearly constant as depicted in Fig. 15. It can be shown that the approximation error $\varepsilon^{(v)}$ from (35) reveals a similar behavior to the eigenvalues. That means that the approximation error decreases only slowly after a characteristic number of eigenmodes. An approximation with more than $v = 20$ eigenvectors is not useful. An interesting point is that the eigenvalues occur in pairs or triples several times.

As mentioned above, the dynamics can be represented in a subspace $U^{(v)}$, which is the span of the first v eigenvectors

$$\tilde{\mathbf{u}}^{(v)} = \bar{\mathbf{u}} + \sum_{i=1}^{v} a_i(t)\,\boldsymbol{\psi}_i, \quad \tilde{\mathbf{u}}^{(v)}\in U^{(v)} = \operatorname{span}\{\boldsymbol{\psi}_1,\ldots,\boldsymbol{\psi}_v\}. \tag{44}$$

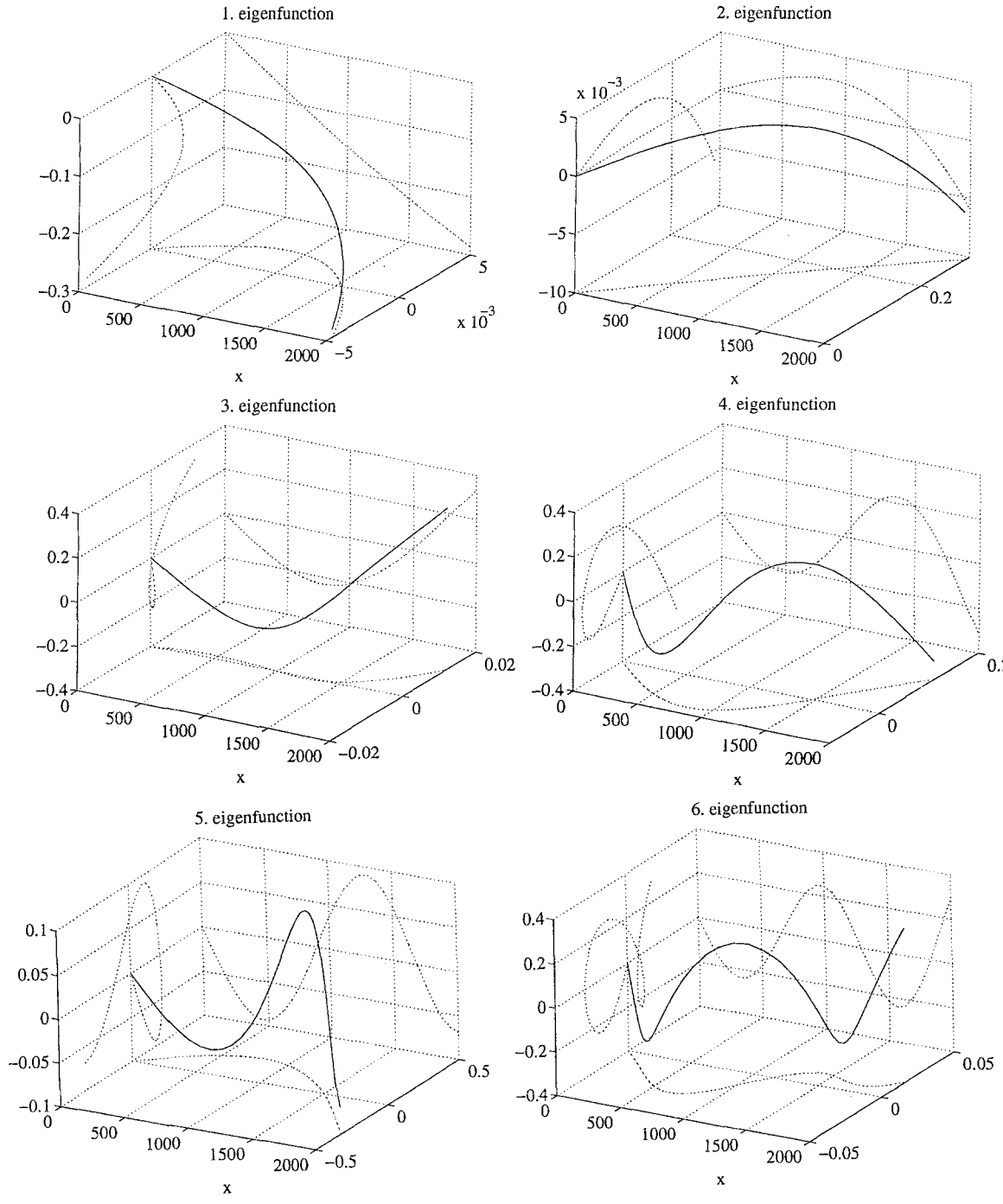

Fig. 12. First six eigenvectors of the torsional vibrations of the drill string in state space from POD for $\omega_0 = 10.1$ rad/s and $l = 2000$ m

Inserting (44) in the system Eqs. (41) yields

$$\dot{\mathbf{u}} = \mathbf{A}^{\star}\left[\bar{\mathbf{u}} + \sum_{i=1}^{v} a_i(t)\,\boldsymbol{\psi}_i\right] + \mathbf{f}^{\star}\left[\bar{\mathbf{u}} + \sum_{i=1}^{v} a_i(t)\,\boldsymbol{\psi}_i\right]. \tag{45}$$

Multiplying (45) from the left-hand side with $\boldsymbol{\psi}_j$, and applying the orthogonality condition (32) leads to a set of v ODEs for the v time functions $a_i(t)$

$$\dot{a}_j = \boldsymbol{\psi}_j^T\bar{\mathbf{u}} + \sum_{i=1}^{v} a_i\boldsymbol{\psi}_j^T\mathbf{A}^{\star}\boldsymbol{\psi}_i + \boldsymbol{\psi}_j^T\,\mathbf{f}^{\star}\left[\bar{\mathbf{u}} + \sum_{i=1}^{v} a_i(t)\,\boldsymbol{\psi}_i\right], \tag{46}$$

$$= c_j + \sum_{i=1}^{v} a_i b_{ij} + f_j^{\star\star}(a_1,\ldots,a_v), \quad j = 1,\ldots,v, \tag{47}$$

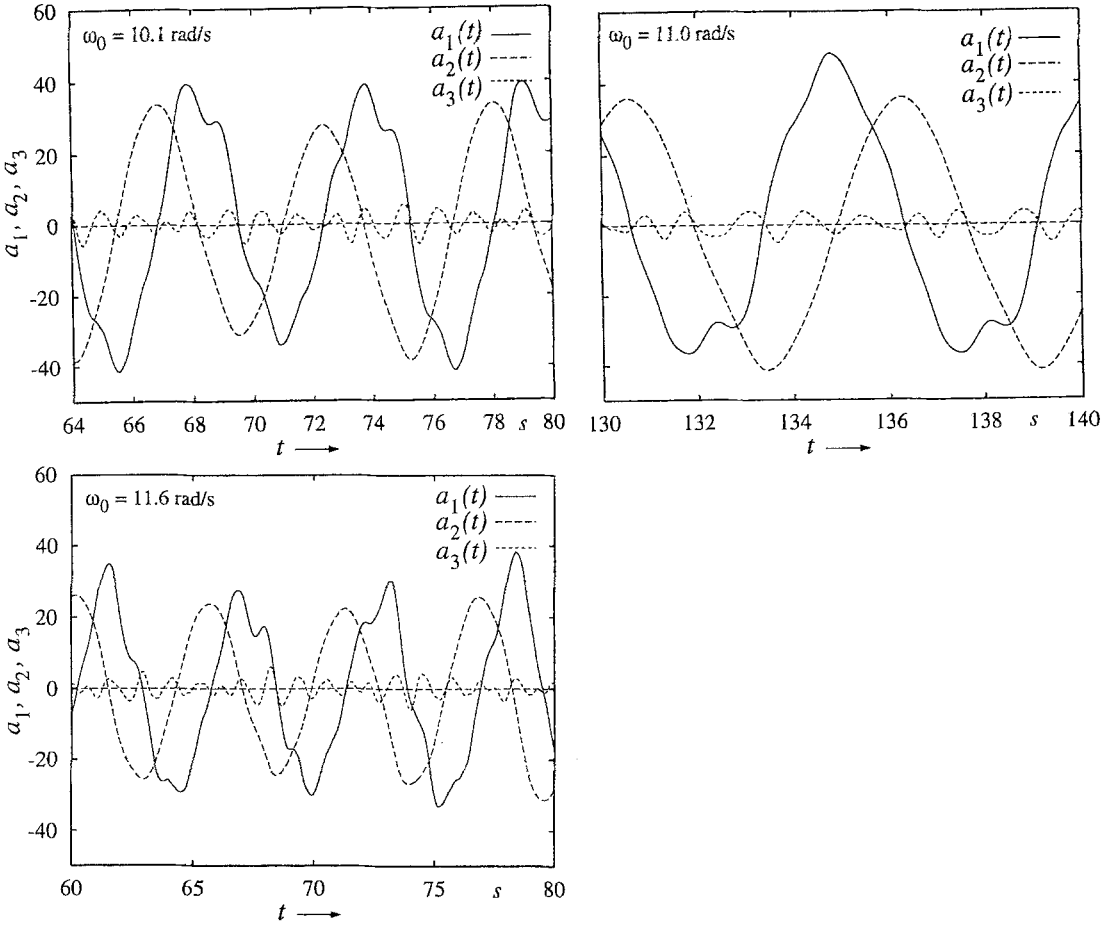

Fig. 13. Time functions a_i, $i = 1,\ldots,3$ for different values of the bifurcation parameter $\mu = \omega_0$

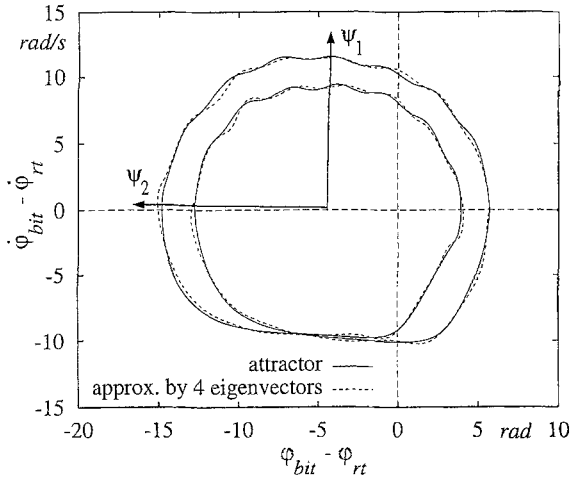

Fig. 14. Orientation of the first two eigenvectors in the state space of the bit in a co-rotating coordinate frame

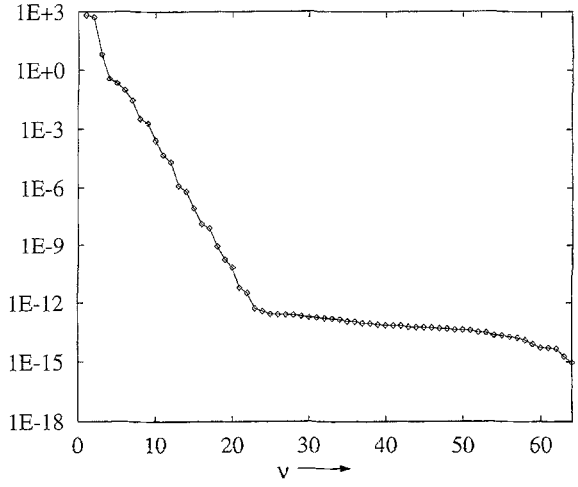

Fig. 15. Eigenvalues of the eigenvectors

where

$$c_j = \boldsymbol{\psi}_j^T \bar{\mathbf{u}}, b_{ij} = \boldsymbol{\psi}_j^T \mathbf{A}^* \boldsymbol{\psi}_i, \mathbf{f}_j^{**} = \boldsymbol{\psi}_j^T \mathbf{f}^*.$$

In order to solve the ν ODEs given in (46), ν initial conditions are necessary

$$a_j(0) = \boldsymbol{\psi}_j^T(\mathbf{u}_0 - \bar{\mathbf{u}}) = c_{0j} - c_j, \quad j = 1,\ldots,\nu. \tag{48}$$

The dimension of the system $2n$ can be reduced by POD to the level of v. Looking at the distribution of the eigenvalues, Fig. (15), typically $v = 20$ eigenvectors give a good approximation. The reduction factor is $\rho = 2n:v = 130:20 = 6.5:1$, which is 15% of the system's original dimension.

5
Conclusions

An analysis of the spatio-temporal dynamics of long torsional strings by means of proper orthogonal decomposition has been presented for the first time. After introducing a string model, we have described the mathematical model used in the subsequent sections. We have outlined the problems with rotating coordinate frames, discussed the properties of the proper orthogonal decomposition in a readily comprehensible way, and demonstrated how to analyze a mechanical system by means of it. The advantages of efficient approximation and powerful system dimension reduction have been presented.

References

1. **Armbruster, D.:** Analyzing spatio-temporal complexity. In: Kreuzer, E.; Schmidt, G. (eds.) 1st European Nonlinear Oscillations Conference, pp. 1–21. Berlin: Akademie Verlag 1993
2. **Aubry, N.; Guyonnet, R.; Lima, R.:** Spatiotemporal analysis of complex signals: Theory and applications. J. Stat. Phys. 64 (1991) 638–739
3. **Berkooz, G.; Holmes, P.; Lumley, J. L.:** The proper orthogonal decomposition of turbulent flows. Annu. Rev. Fluid Mech. 25 (1993) 539–575
4. **Finnie, I.; Bailey, J. J.:** An experimental study of drill-string vibration. Trans. ASME Ser. B: J. Eng. Indust. 82 (1960) 129–135
5. **Golub, G. H.; Van Loan, Ch. F.:** Matrix computations (2nd ed.) Baltimore: The Johns Hopkins University Press (1989)
6. **Karhunen, K.:** Zur Spektraltheorie stochastischer Prozesse. Ann. Acad. Sci. Fenn. Series A-I. Mathematica 34 (1946)
7. **Karhunen, K.:** Über lineare Methoden in der Wahrscheinlichkeitsrechnung. Ann. Acad. Sci. Fenn. Series A-I. Mathematica 37 (1947)
8. **Kirby, M.; Armbruster, D.:** Reconstructing phase space from pde simulations. Z. Angew. Math. Phys. 43 (1992) 999–1022
9. **Kreuzer, E.:** Numerische Untersuchung nichtlinearer dynamischer Systeme. Berlin: Springer 1987
10. **Loève, M.:** Functions aléatoires de second ordre. C. R. Acad. Sci. 220 (1945)
11. **Loève, M.:** Probability theory (4th ed.) New York: Springer 1978
12. **Sirovich, L.:** Turbulence and the dynamics of coherent structures. Part I–III. Quart. Appl. Math. 45 (1987) 561–590
13. **Smith, G. D.:** Numerical solution of partial differential equations: Finite difference methods. Oxford: Clarendon Press 1985
14. **Troger, H.; Steindl, A.:** Nonlinear stability and bifurcation theory. New York: Springer 1991
15. **Vemuri, V.; Karplus, W. J.:** Digital computer treatment of partial differential equations. Englewood Cliffs: Prentice-Hall 1981